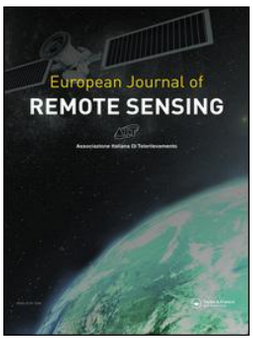

European Journal of Remote Sensing

ISSN: (Print) 2279-7254 (Online) Journal homepage: https://www.tandfonline.com/loi/tejr20

Downscaling Landsat Land Surface Temperature over the urban area of Florence

Stefania Bonafoni, Roberta Anniballe, Beniamino Gioli & Piero Toscano

To cite this article: Stefania Bonafoni, Roberta Anniballe, Beniamino Gioli & Piero Toscano (2016) Downscaling Landsat Land Surface Temperature over the urban area of Florence, European Journal of Remote Sensing, 49:1, 553-569, DOI: 10.5721/EuJRS20164929

To link to this article: https://doi.org/10.5721/EuJRS20164929

Published online: 17 Feb 2017.

European Journal of Remote Sensing - 2016, 49: 553-569
doi: 10.5721/EuJRS20164929
Received 22/03/2016 accepted 28/07/2016

European Journal of Remote Sensing
An official journal of the Italian Society of Remote Sensing

www.aitjournal.com

Downscaling Landsat Land Surface Temperature over the urban area of Florence

Stefania Bonafoni[1]*, Roberta Anniballe[2], Beniamino Gioli[3] and Piero Toscano[3]

[1]Department of Engineering, University of Perugia, via G. Duranti 93, 06125 Perugia, Italy
[2]Department of Information Engineering, Electronics and Telecommunications, Sapienza University of Rome, via Eudossiana 18, 00184 Roma, Italy
[3]Institute of Biometeorology (IBIMET - CNR), via G. Caproni 8, 50145 Firenze, Italy
*Corresponding author, e-mail address: stefania.bonafoni@unipg.it

Abstract
A new downscaling algorithm for land surface temperature (LST) images retrieved from Landsat Thematic Mapper (TM) was developed over the city of Florence and the results assessed against a high-resolution aerial image. The Landsat TM thermal band has a spatial resolution of 120 m, resampled at 30 m by the US Geological Survey (USGS) agency, whilst the airborne ground spatial resolution was 1 m. Substantial differences between Landsat USGS and airborne thermal data were observed on a 30 m grid: therefore a new statistical downscaling method at 30 m was developed. The overall root mean square error with respect to aircraft data improved from 3.3 °C (USGS) to 3.0 °C with the new method, that also showed better results with respect to other regressive downscaling techniques frequently used in literature. Such improvements can be ascribed to the selection of independent variables capable of representing the heterogeneous urban landscape.
Keywords: Land surface temperature, urban area, airborne data, Landsat images, downscaling.

Introduction
Land surface temperature (LST) is a fundamental variable controlling the surface energy balance, and it is involved in physical, chemical, and biological processes of the Earth surface. In urban areas, LST allows the assessment of the surface urban heat island (SUHI) effect [Oke, 1973; Oke, 1982; Voogt, 2004]. Earth observation data have been widely exploited to retrieve LST: spaceborne sensors have the advantages of covering large areas at the same time, while temperature observations registered *in situ* are unevenly distributed in space. Different spaceborne platforms, such as ASTER [Hartz et al., 2006; Lu and Weng, 2006; Weng et al., 2014], AVHRR [Lee, 1993; Streutker, 2003; Stathopoulou and Cartalis, 2009], MODIS [Pou et al., 2006; Anniballe at al., 2014] and Landsat [Xian and Crane, 2006; Yuan and Bauer, 2007; Xu et al., 2009; Xiong et al., 2012], were used to retrieve the SUHI.

Different factors need to be quantified to retrieve LST from satellite thermal infrared data, including sensor radiometric calibration, atmospheric correction and surface emissivity selection. These factors greatly influence the final result, thus estimation of uncertainties in the retrieval process and validation procedures are important tasks especially for operational datasets. Moreover, the satellite sensor spatial resolution may be a limiting factor in representing the fine scale spatial variability of LST, especially in the presence of impervious surfaces and sharp transitions (e.g., buildings, roads, parking lots, sidewalks, and other built surfaces), such as in urban areas. Recommendations on the optimal spatial resolution for a satellite mission aimed at analyzing the urban LST and the related SUHI effects were suggested by [Sobrino et al., 2012], finding that resolutions finer than 50 m are necessary to successfully monitor the SUHI effect at district level and to avoid temperature underestimation. Lower spatial resolutions do not generally allow to distinguish thermal variations among nearby zones inside the city.

Besides satellites, airborne sensors may also be used to measure the thermal properties of the surface. The benefits of aircraft thermal remote sensing are a much higher spatial resolution (down to sub-meter) and the possibility to plan surveys when conditions are optimal to meet the project requirements. On the other hand, aircraft surveys are necessarily sporadic and expensive, and cannot therefore represent an operational solution on a continuous basis. Using light aircraft with low weight and low cost sensors can represent a compromise between operational costs, data coverage and accuracy. Airborne thermal remote sensing has been utilized in some studies for the monitoring of the SUHI effects [Lo et al., 1997; Voogt and Oke, 1998; Saaroni et al., 2000; Gluch et al., 2006; Kottmeier et al., 2007].

In this work, we developed a new downscaling algorithm for Landsat TM LST from 120 to 30 m spatial resolution, and validated it against high-resolution (1 m pixel size) airborne LST imagery over the city of Florence. The improvement associated with the 30 m sharpening approach was quantified, and compared with the USGS standard 30 m resampled product currently available.

In addition, a comparison with other downscaling techniques based on regression schemes was carried out in order to further evaluate the performance of the new method. The satellite data capability to resolve spatial thermal details was assessed given the availability of a unique high-resolution airborne imagery, since *in situ* measurements, sparsely distributed, are typically not usable to this aim in heterogeneous urban landscapes.

Study area and data

Study area

The study area is a zone over Florence, Italy (between 43.754 °N to 43.796 °N and 11.226 °E to 11.291 °E), comprising the city center, part of the Arno river and some periurban vegetated areas (Fig. 1), with 31% of vegetation cover. The city is lying in central Italy, having a sub-Mediterranean climate with a hot, dry summer, a mild and quite wet winter, and wet autumn and spring. The city centre is characterized by small squares surrounded by a network of narrow streets linked to the ancient gates; buildings have an average height of 20 m with a maximum height of 116 meters for the Cathedral. The roof style is uniform and made of red terracotta tiles, while large paving stones are still characterizing squares and pedestrian areas.

Landsat data and processing

Data from TM instrument onboard Landsat-5 platform were used, selecting two passages over Florence on July 10 and July 26, 2010, both at 11:50 CEST (Central European Summer Time). These are the two Landsat acquisitions closer to the aircraft flight. The Landsat TM sensor is composed by seven bands, six of them in the visible and near infrared (TM1-5, TM7), and one band in the thermal infrared region, with spectral range 10.4-12.5 μm (TM6). TM has a native spatial resolution of 30 m for the six reflective bands and 120 m for the thermal band. TM6 is also delivered at 30 m, after resampling with a cubic convolution, by the USGS (http://earthexplorer.usgs.gov).

The two images, composed of 160×170 pixels at 30 m resolution, were processed according to the calibration technique proposed by [Chander et al., 2009] in order to convert digital number values to at-sensor spectral radiance values. Atmospheric correction of the TM reflective bands and computation of the surface reflectance were performed using the Chavez method [Chavez, 1996], that requires only data from the same satellite scenes, without needing contemporary in-situ measurements [Cui et al., 2014].

Airborne data and processing

Aircraft measurements were made by a Sky Arrow ERA (Environmental Research Aircraft), that allows the mounting of multiple optic systems [Gioli et al., 2006]. The thermographic images were provided by a FLIR A40-M thermal camera (Tab. 1). The flight survey was made on July 18, 2010 at 13:30 CEST, at 1370 m above sea level, acquiring a total of 305 images with 1 m pixel size over the study area (Fig. 1). These raw images were initially analyzed by the FLIR ThermaCam Researcher Software, then geometrically corrected by means of Ground Control Points and a Digital Elevation Model, finally orthorectified with the PCI Geomatica software. The study area resulted composed of 4815×5115 pixels.

Table 1 - The FLIR A40-M thermal camera main specifications.

Detector	**Uncooled micro bolometer - Vanadium Oxide (VOx)**
Spectral Response Band	7.5-13 μm
Thermal sensitivity	0.08°C at 30°C
IFOV	1.3 mrad
Calibration source	Internal
Focal length	18 mm

Visible images were also simultaneously acquired during the flight by means of a Canon EOS-20D camera allowing a direct comparison with thermographic images. Both airborne and Landsat data were projected in the UTM WGS84 coordinate system.

Ground-based measurements were made at the Ximeniano Observatory, located in the city centre, where meteorological variables are measured continuously. LST of the building roof (Lat 43.774° N, Lon 11.255° E) was acquired using an infrared thermometer (IRT L4000, Everest Interscience), allowing airborne data calibration.

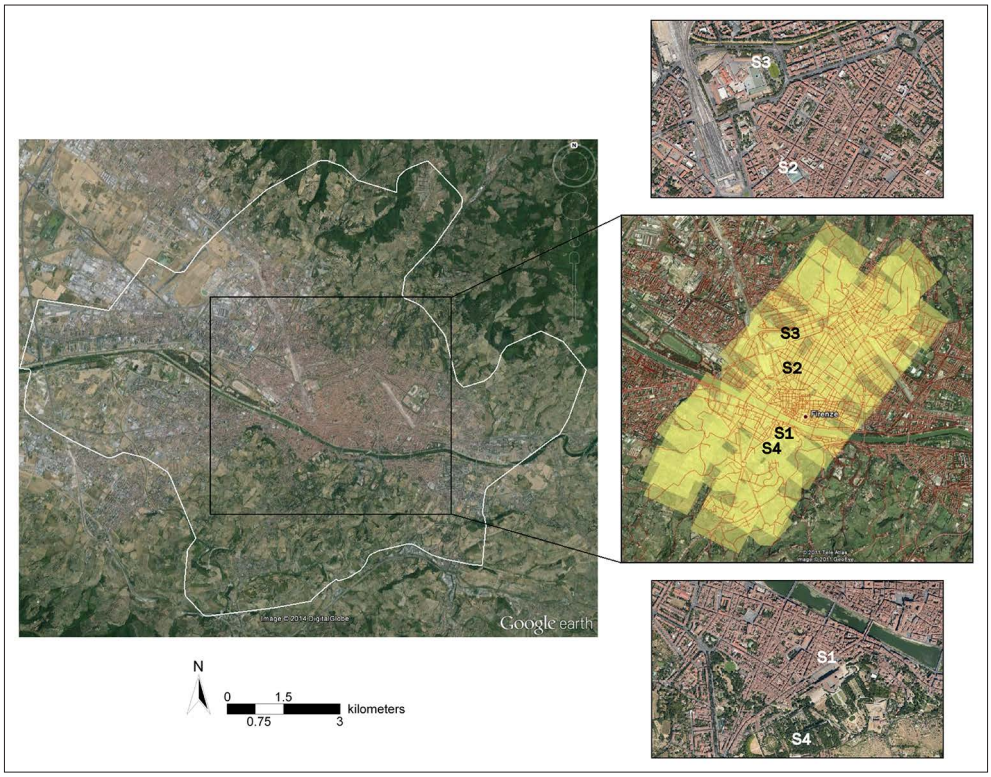

Figure 1 - Study area maps: the white curve (left panel) contains the municipality of Florence (102.3 km²), the yellow zone (right panel) is the study area mapped by the flight (approximately 6 km×2.5 km). S1, S2, S3 and S4 refer to sub-areas analyzed in detail hereafter. Coordinates (UTM WGS84) of the center of the left panel: 680950 m E, 4850000 m N, 32 T zone. Images from Google Earth.

LST data processing

LST retrieval from Landsat

LST was retrieved from the TM6 data, by inverting the radiative transfer equation according to:

$$L_{(sens,\lambda)} = \left[\varepsilon_\lambda B_\lambda \left(T_s \right) + \left(1 - \varepsilon_\lambda \right) L_\lambda^{\downarrow} \right] \tau_\lambda + L_\lambda^{\downarrow} \qquad [1]$$

where $L_{sens,\lambda}$ is the at-sensor radiance at the top-of-atmosphere, ε_λ is the surface emissivity, $B_\lambda(T_s)$ is the Planck's law where T_s is the LST, $L_\lambda^{\downarrow}$ is the downwelling atmospheric radiance, τ_λ is the total atmospheric transmissivity and $L_\lambda^{\downarrow}$ is the upwelling atmospheric radiance. From Equation [1] it is possible to find LST by inversion of the Planck's law [Jimenez-Munoz et al., 2009], known the surface emissivity and the atmospheric parameters τ_λ, $L_\lambda^{\downarrow}$ and $L_\lambda^{\downarrow}$. These atmospheric parameters were computed using a web-based tool (http://atmcorr.gsfc.nasa.gov) that takes the National Centers for Environmental Prediction

modeled atmospheric profiles as inputs to the MODTRAN radiative transfer code [Barsi et al., 2003; Barsi et al., 2005] for a given site and date [Coll et al., 2010].
Land surface emissivity ε_λ, was estimated using a Normalized Difference Vegetation Index (NDVI) method [Sobrino et al., 2004]: from the NDVI image, natively at 30 m spatial resolution, the fractional vegetation cover (f_v) was computed and inserted in the effective emissivity equation [Stathopoulou and Cartalis, 2009]:

$$\varepsilon_\lambda = (1 - f_v)\varepsilon_c + f_v\varepsilon_v \quad [2]$$

where ε_v is the emissivity of vegetation (0.99) and ε_c is the emissivity of the urban/densely built surfaces (0.94). Pixels corresponding to water surfaces (e.g. the Arno river) were settled to 0.99. Such emissivity values were chosen in agreement with [NASA, 1999; Hancock et al., 2012] considering the TM6 spectral range (10.4-12.5 μm).
An additional emissivity estimation approach was also tested, consisting in a subpixel-level land cover classification based on a spectral mixture analysis (SMA) [Mitraka et al., 2012], that resulted in a RMS emissivity difference SMA-NDVI of 0.018 and a RMS LST difference of 1.1°C. Such LST difference was considered not influential for the purpose of this work, therefore the NDVI approach was adopted. Overall, LST was retrieved using the TM6 data resampled at 30 m from the original 120 m, using the emissivity map generated with NDVI data that are natively at 30 m resolution.

LST retrieval from airborne data

Equation [1] was also employed at the aircraft altitude [Jimenez-Munoz et al., 2012] to retrieve LST from airborne thermal data. The same emissivity algorithm used for the Landsat LST retrieval was applied. Since it was not possible to use the above web-based tool for aircraft altitude and spectral range, the atmospheric correction of the airborne radiances was applied following a tuning approach. Different values of the atmospheric parameters τ_λ, $L_\lambda^{\downarrow}$ and $L_\lambda^{\downarrow}$ were generated and a triplet was chosen according to the *in situ* LST value registered by the infrared thermometer at the ground: the selected triplet minimized the error between the aircraft LST 1 m^2 pixel covering the ground reference roof and the measured *in situ* value, obtaining a difference of 0.5°C. Such an empirical estimation of the atmospheric parameters is possible by the complete match between aircraft pixel and the ground infrared thermometer field of view area.

Downscaling framework

A downscaling is the enhancement of spatial resolution of an imagery data using information available at a higher spatial resolution, finally increasing the information content of the original image [Atkinson, 2013]. In this work Landsat LST was downscaled from 120 to 30 m resolution, using the 30 m reflective bands in a regressive disaggregation approach [Kustas et al., 2003; Dominguez et al., 2011; Mukhherjee et al., 2015]. Several approaches using NDVI at finer resolution for LST downscaling were proposed [Kustas et al., 2003; Agam et al., 2007; Inamdar et al., 2008; Mukhherjee et al., 2015], even though NDVI cannot entirely explain LST spatial variations, especially in urban texture. Since an urban area is a complex system composed of heterogeneous features, three generalized land cover

classes, i.e. built-up, vegetation and open water, were considered here. NDVI, Normalized Difference Built-up Index (NDBI), and Normalized Difference Water Index (NDWI) were computed from Landsat data to represent those three classes [Xu, 2007; Borgogno-Mondino et al., 2016]:

$$NDVI = (TM4 - TM3) / (TM4 + TM3) \quad [3]$$

$$NDBI = (TM5 - TM4) / (TM5 + TM4) \quad [4]$$

$$NDWI = (TM2 - TM4) / (TM2 + TM4) \quad [5]$$

The proposed downscaling approach is based on fitting a least-squares linear relation using these three spectral indices as predictors and LST as the predicted variable, after the aggregation of each spectral index to 120 m resolution with block-averaging (subscript 120):

$$LST_{120} = a_0 + a_1 \cdot NDVI_{120} + a_2 \cdot NDBI_{120} + a_3 \cdot NDWI_{120} \quad [6]$$

Then, a residual of LST (ΔT_{120}) is computed as the difference between model estimation (LST_{120}) and the corresponding observation (LST_{obs}) [Kustas et al., 2003]:

$$\Delta T_{120} = LST_{obs} - LST_{120} \quad [7]$$

The residual ΔT_{120} is introduced in the model to take into account part of LST spatial variability that depends on factors other than the employed predictors, such as soil moisture. Finally, finer resolution LST is estimated by:

$$LST_{30} = a_0 + a_1 \cdot NDVI_{30} + a_2 \cdot NDBI_{30} + a_3 \cdot NDWI_{30} + DT_{120} \quad [8]$$

where the coarse resolution regression coefficients are applied to finer spatial resolution spectral indices, adding the residual error of the corresponding coarse resolution image to increase the accuracy. Multiple regressions comprising powers of predictors (a n*th* order polynomial regression) were also considered [Bonafoni, 2016], inserting the powers in a step-wise mode. Moreover other vegetation indices instead of NDVI [Bonafoni, 2015] were evaluated, but the results were quite similar. The lower root mean square error (RMSE) between estimates and aircraft LST was obtained by the model:

$$LST_{30} = a + b \cdot NDVI_{30} + c \cdot (NDVI_{30})^2 + d \cdot NDBI_{30} + e \cdot (NDBI_{30})^2 + f \cdot (NDWI_{30}) + g \cdot (NDWI_{30})^2 + DT_{120} \quad [9]$$

The performance of this custom downscaling model was compared with the USGS cubic convolution method.

Results and discussion

Figure 2 reports the LST images of Florence study area retrieved by spaceborne and airborne sensors. For comparison purposes, the images were gridded with a resolution of 30 m: however, the native 1 m resolution airborne images will be always considered to preserve the information content of the high resolution map. Besides the two individual Landsat images acquired on 10th and 26th of July 2010, their pixel-by-pixel average was also computed (Fig. 2d).

Overall, excluding some differences in detailing specific spatial features, the LST spatial patterns are similar: lower temperatures were registered in water bodies and vegetation areas, while higher values were observed in the central urbanized areas, as expected. Clear differences emerge in the detail definition due to the different native spatial resolution of the Landsat TM and airborne sensors.

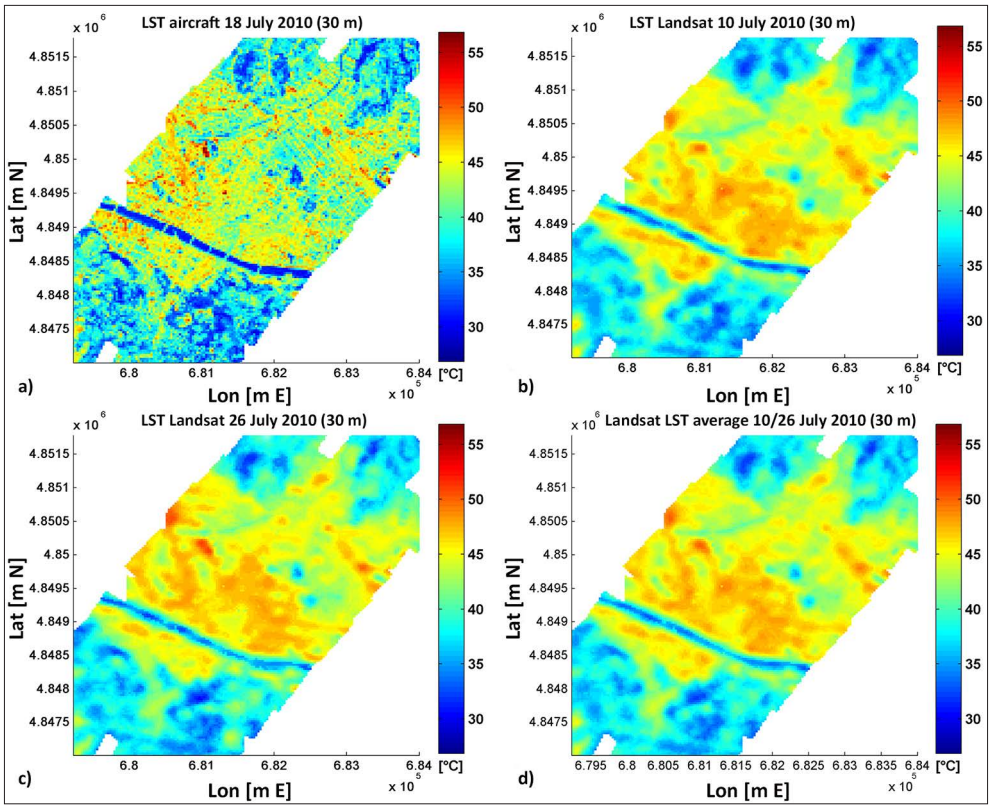

Figure 2 - a) LST [°C] full image from airborne data (18th July 2010) with 30 m averaged pixels; b) LST [°C] from Landsat (10th July 2010); c) LST [°C] from Landsat (26th July, 2010); d) LST [°C] from Landsat (average of 10th and 26th July). Landsat pixels are 30×30 m from the USGS. Lat/Lon are in UTM, 32 T zone.

A detailed analysis for restricted sub-areas of the city containing different land cover types (S1 to S4, Fig. 1) was made: Figure 3a show the sub-area S1.

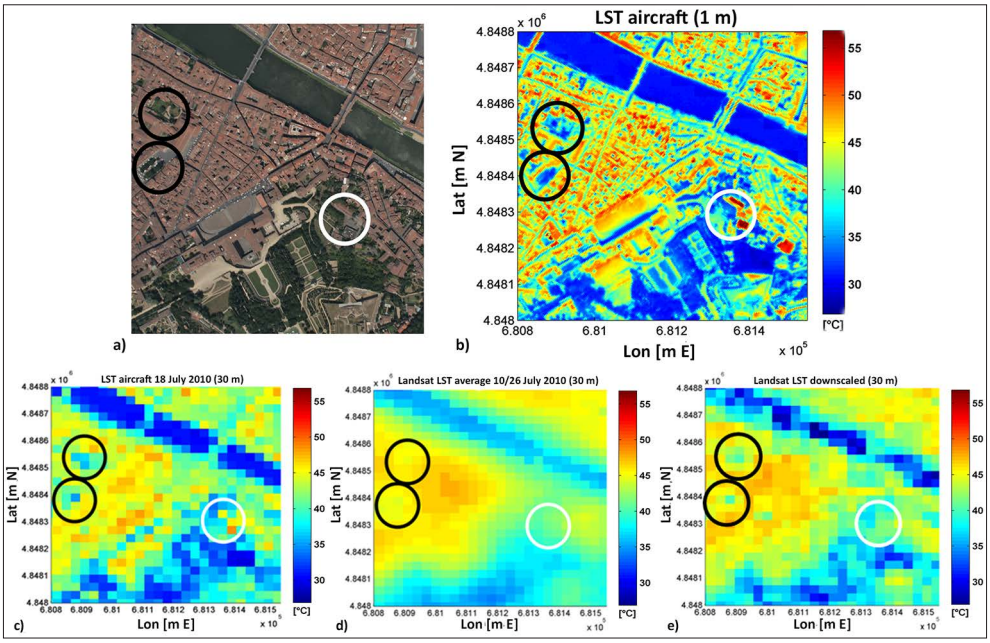

Figure 3 - Sub-area S1 (750×800 m). a) Visible image from aircraft; b) LST from airborne data with 1 m resolution; c) LST [°C] from airborne data with 30 m averaged pixels; d) LST [°C] from Landsat resampled by the USGS at 30 m; e) LST [°C] from Landsat downscaled at 30 m. The white circle refers to a strong heating of a roof among the vegetation, the black circles to vegetated/shadowed cold zones among the built-up area.

The pixels within the white circle of Figure 3, referred to a strong heating, lead to a difference (Landsat USGS-aircraft) around -10°C. This large negative difference is ascribed to the different spatial resolution of the sensor acquisitions, where the TM6 120 m footprint averages the hot spot with the surrounding colder vegetation. The pixels inside of the two black circles refer instead to large positive differences due to the inability of the Landsat TM to detect restricted vegetated or shadowed cold zones. Just on the right of the black circles, where a homogeneous area of terracotta tiled roofs is present (Fig. 3a), the LST difference decreases. It is important to point out how the airborne 30 m image (Fig 3c) clearly preserves these thermal discontinuities, if compared with the 1-m image (Fig. 3b). Figure 3d demonstrates that the 30 m resample procedure of TM6 data performed by the USGS is not well capable to resolve spatial details. Even the use of the emissivity map generated employing native NDVI 30 m data does not improve this drawback. Figure 3e shows the new downscaled map for sub-areas S1. The downscaled image appears more detailed, well resolving tree foliage and vegetation canopy in the lower part of the scene, with colder LST pixels. In the USGS image (Fig. 3d) a more uniform pattern is present. Also the colder vegetated pixels (black circles in Fig. 3) are better recognized in the downscaled image. The

very warm single pixel inside the white circle is not recovered, since it represents a small size hot-spot not present in the data training of the regression scheme. The transition pixels of the Arno riverside present some problems, whilst the use of the water index NDWI in the regression produces a cooling of the water pixels with respect to the USGS ones, that overall improves the agreement with aircraft observations (Fig. 3c).
Sub-area S2 is characterized by a large and hot roof surrounded by shadowed cooler areas (Fig. 4a and 4b). Those thermal differences are still detected in the 30 m averaged airborne image (Fig 4c) while they are almost dissolved in the satellite USGS images (Fig. 4d).

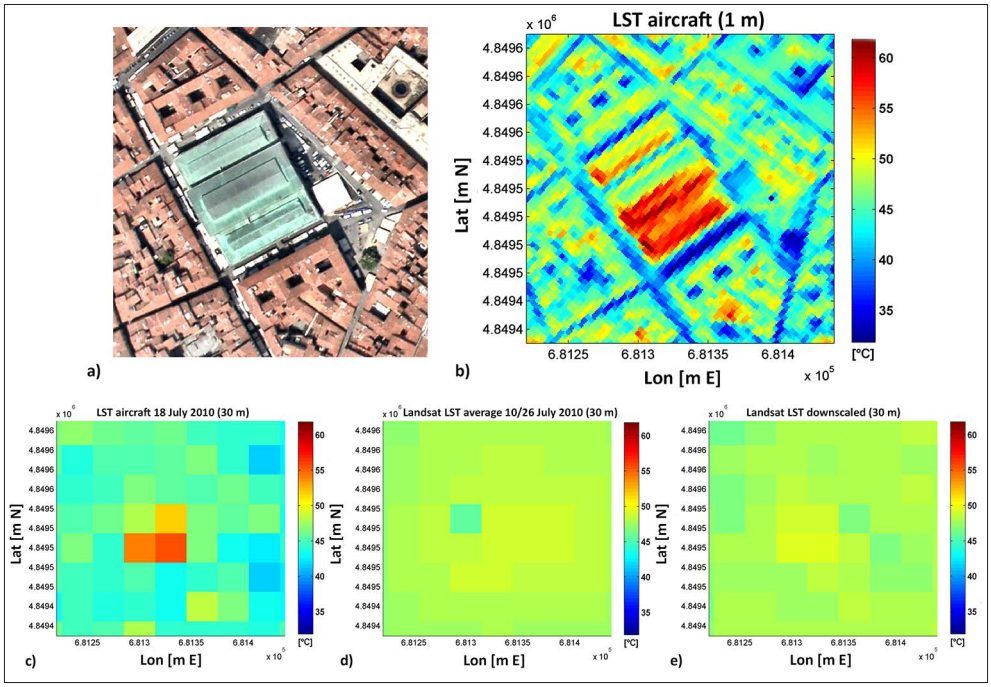

Figure 4 - Sub-area S2 (220×220 m). a) Visible image from aircraft; b) LST from airborne data with 1 m resolution; c) LST [°C] from airborne data with 30 m averaged pixels; d) LST [°C] from Landsat resampled by the USGS at 30 m; e) LST [°C] from Landsat downscaled at 30 m.

The downscaling (Fig. 4e) does not provide significant improvements, since the material of the heated roof is not associated to any variation of the three selected spectral indices.
Sub-area S3 is focused on the contrast between a cool urban water surface and an adjacent large hot roof (Fig. 5a and 5b), representing another example exhibiting large differences between satellite and airborne images. The Landsat USGS image (Fig. 5d) reveals the inability to detect hot and cold thermal peaks that are instead present in the 30 m airborne image (Fig. 5c).

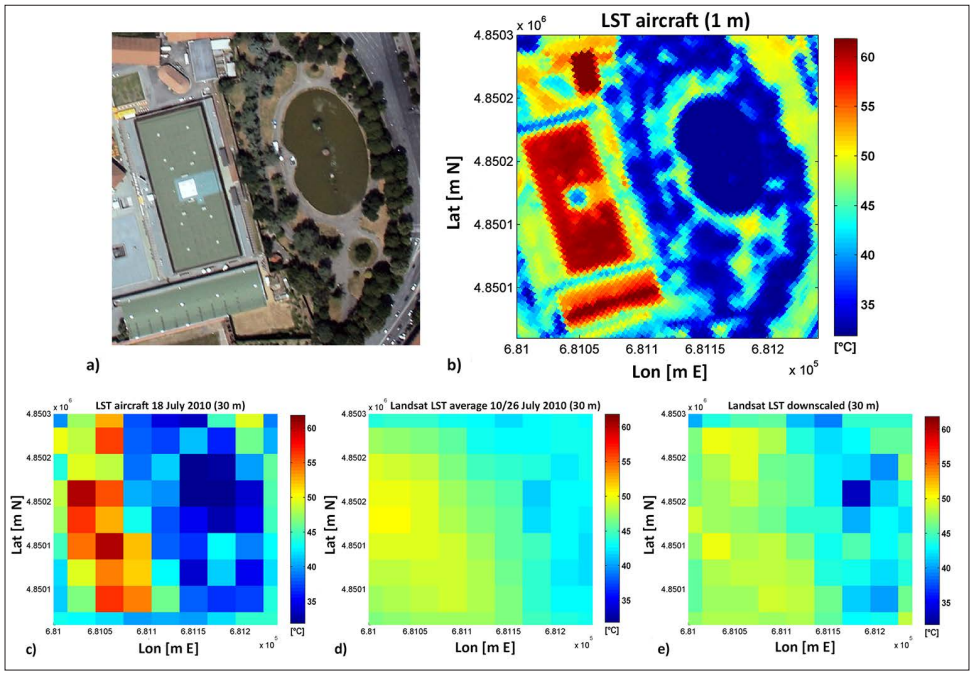

Figure 5 - Sub-area S3 (240×240 m). a) Visible image from aircraft; b) LST from airborne data with 1 m resolution; c) LST [°C] from airborne data with 30 m averaged pixels; d) LST [°C] from Landsat resampled by the USGS at 30 m; e) LST [°C] from Landsat downscaled at 30 m.

Instead, in the right part of the scene an improvement in the downscaled image is clearly observed (Fig. 5e).

Sub-area S4 represents a homogeneous vegetated land (Fig. 6a). As expected, in such conditions the LST difference between Landsat and airborne becomes low even for USGS resample (Fig. 6b).

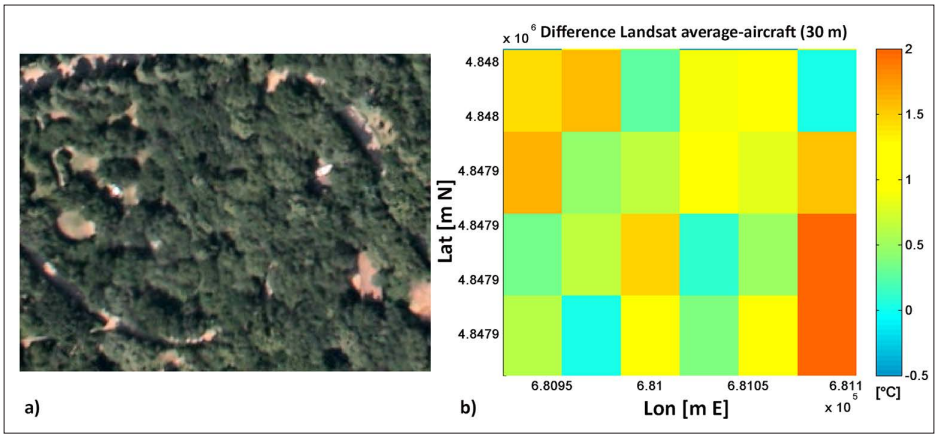

Figure 6 - Sub-area S4 (180×120 m). a) visible image from aircraft; b) LST [°C] difference (Landsat USGS average-aircraft).

Besides the visual inspection, the benefit to employ a custom downscaling method was evaluated from a quantitative standpoint considering the whole image. The RMSE with respect to aircraft LST improves from 3.3°C (USGS) to 3.0°C (downscaled). In Figure 7 the distribution of LST difference for both USGS and downscaled images is shown.

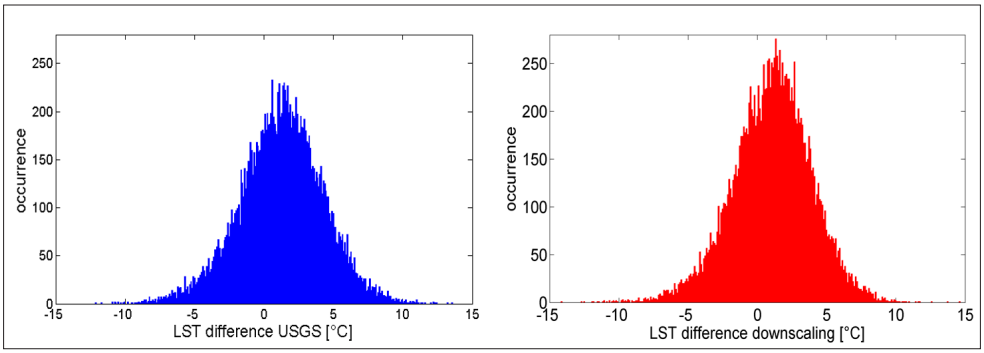

Figure 7 - Distribution of LST difference [°C] between aircraft and Landsat images (downscaled, red, and from USGS, blue).

Mean (m) and standard deviation (σ) of the error distribution are:

m =1.25°C; σ =3.02°C for USGS-aircraft LST comparison;

m =1.03°C; σ = 2.86°C for downscaling-aircraft LST comparison.

Some pixels with high errors persist in the downscaled image, but the improvement in some areas is appreciable as qualitatively shown in the above sub-areas. To explore the downscaling performance in relation to the urban texture, the RMSE for pixels belonging to different land cover classes was evaluated. Three classes (built-up, vegetation and open water) were selected using the NDVI, NDBI and NDWI indices, settling a conservative index threshold based also on a visual inspection. An additional class of "mixed" pixels, not belonging to the previous three classes, was considered. Table 2 reports the RMSE comparing USGS and downscaled LST with respect to aircraft data.

Table 2 - RMSE [°C] of USGS and downscaled LST with respect to aircraft LST for the four land cover classes (built-up area, vegetation, water, mixed).

Class	Index threshold	RMSE [°C] (USGS)	RMSE [°C] downscaling
built-up area	NDBI > 0.0	3.12	3.11
vegetation	NDVI > 0.6	3.11	2.77
water	NDWI >- 0.1	3.82	3.25
mixed	complementary pixels	3.64	3.09

The results point out the noticeable improvement of the downscaled LST for the mixed, water and vegetation classes. An assessment of the custom method accuracy with respect to statistical downscaling techniques based on regression and frequently used in literature

is proposed. The DisTrad method [Kustas et al., 2003], using only NDVI as independent variable, the TsHARP method [Agam et al., 2007] using the fractional vegetation cover (fc), and the HUTS method [Dominguez et al., 2011], including albedo as independent variable, were considered for comparison purpose. Table 3 summarizes the results in terms of RMS error with respect to aircraft LST.

Table 3 - LST RMSE [°C] with respect to aircraft image of the proposed method and other statistical downscaling methods.

Method	RMSE (°C)
DisTrad: a +b·NDVI+ c·$(NDVI)^2$	3.20
TsHARP: a +b·fc	3.19
HUTS: function(NDVI, albedo)	3.42
Custom method (Eq. 9)	3.01

The proposed approach shows superior performance since the selected independent variables are more suitable to explain heterogeneous urban features. Therefore, a custom selection of predictors in the multiple regression scheme can improve the sharpening accuracy of a specific area.

As a further analysis, Pearson correlation coefficient (r) was adopted as a performance metric to compare custom and USGS sharpening schemes against airborne images across a range of spatial resolutions (Fig. 8). The custom downscaled image exhibits a better correlation with the aircraft image than the USGS one until 120 m. Both curves, after a sharp increase from 30 m to 150 m resolution, basically level off to an average value r = 0.95 approaching the 420 m resolutions.

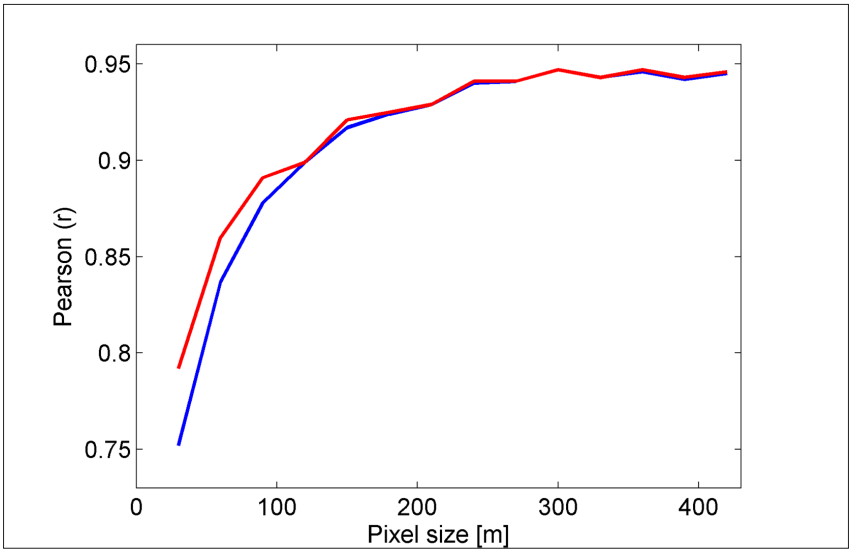

Figure 8 - Pearson correlation coefficient between aircraft and Landsat images (downscaled, red curve, and from USGS, blue curve). For each sample resolution the images were block-averaged to reach the same pixel size, ranging from 30 m to 420 m.

Our results confirm that even the use of resolved surface properties to classify urban regions cannot improve the satellite capability to resolve some thermal details. Nevertheless, the custom downscaling procedure provides an additional value by improving the overall RMSE with respect to the USGS image and to other regressive downscaling techniques.

Conclusions

In this work we retrieved LST from Landsat TM over the city of Florence, developed a custom downscaling framework, and analyzed its performances using high-resolution LST airborne imagery. Landsat thermal observations prove to be effective to provide a global pattern of LST over a city area, but its native spatial resolution is not adequate to identify thermal details over a complex texture, calling for the development of adequate downscaling schemes. The proposed sharpening method improves the overall RMSE with respect to other regressive downscaling approaches, pointing out the impact of the predictor selection in a heterogeneous urban texture. However, this method is not always capable of resolving specific thermal details, showing that the image sharpening topic is still an open issue. These results have been assessed thanks to the availability of a high resolution airborne image. Such data 'bridge a gap' between ground truth measurements and satellite observations, since the latter could not be directly compared with *in situ* measurements in heterogeneous urban landscapes. High resolution thermal images, in the next future provided also by small unmanned aerial platforms, will be a resource to build effective downscaling frameworks for satellite observations of SUHI effects.

Acknowledgments

We wish to thank Nicomino Fiscante for the airborne raw image processing, Claudio Belli (Terrasystem) for the flight coordination and data acquisition (www.terrasystem.it), Alessandro Zaldei (CNR IBIMET) for the ground measurements, Enzo Magliulo (CNR ISAFOM) for providing the aircraft platform. Flight surveys were made in the frame of the EC project BRIDGE (www.bridge-fp7.eu).

References

Agam N., Kustas W.P., Anderson M.C., Li F., Neale C.M. (2007) - *A vegetation index based technique for spatial sharpening of thermal imagery*. Remote Sensing of Environment, 107 (4): 545-558. doi: http://dx.doi.org/10.1016/j.rse.2006.10.006.

Anniballe R., Bonafoni S., Pichierri M. (2014) - *Spatial and temporal trends of the surface and air heat island over Milan using Modis data*. Remote Sensing of Environment, 150: 163-171. doi: http://dx.doi.org/10.1016/j.rse.2014.05.005.

Atkinson P.M. (2013) - *Downscaling in remote sensing*. International Journal of Applied Earth Observation and Geoinformation, 22: 106-114. doi: http://dx.doi.org/10.1016/j.jag.2012.04.012.

Barsi J.A., Barker J.L., Schott J.R. (2003) - *An atmospheric correction parameter calculator for a single thermal band earth-sensing instrument*. Proceedings of IEEE International Geoscience and Remote Sensing Symposium, Toulouse, France: 3014-3016. doi: http://dx.doi.org/10.1109/IGARSS.2003.1294665.

Barsi J.A., Schott J.R., Palluconi F.D., Hook S.J. (2005) - *Validation of a web-based atmospheric correction tool for single thermal band instruments*. In: SPIE, Bellingham, WA,

5882. doi: http://dx.doi.org/10.1117/12.619990.

Bonafoni S. (2015) - *The spectral index utility for summer urban heating analysis*. Journal of Applied Remote Sensing, 9 (1): 1-16. doi: http://dx.doi.org/10.1117/1.JRS.9.096030.

Bonafoni S. (2016) - *Downscaling of Landsat and MODIS Land Surface Temperature over the heterogeneous urban area of Milan*. IEEE Journal of Selected Topics in Applied Earth Observations and Remote Sensing, 9 (5): 2019-2027. doi: http://dx.doi.org/10.1109/JSTARS.2016.2514367.

Borgogno-Mondino E., Lessio A., Gomarasca M.A. (2016) - *A fast operative method for NDVI uncertainty estimation and its role in vegetation analysis*. European Journal of Remote Sensing, 49: 137-156. doi: http://dx.doi.org/10.5721/EuJRS20164908.

Chander G., Markham B.L., Helder D.L. (2009) - *Summary of current radiometric calibration coefficients for Landsat MSS, TM, ETM+, and EO-1 ALI sensors*. Remote Sensing of Environment, 113 (5): 893-903. doi: http://dx.doi.org/10.1016/j.rse.2009.01.007.

Chavez P.S. (1996) - *Image-based atmospheric corrections-revisited and improved*. Photogrammetric engineering and remote sensing, 62 (9): 1025-1036. Available online at: http://www.unc.edu/courses/2008spring/geog/577/001/www/Chavez96-PERS.pdf.

Coll C., Galve J.M., Sanchez J.M., Caselles V. (2010) - *Validation of Landsat-7/ETM+ thermal-band calibration and atmospheric correction with ground-based measurements*. IEEE Transaction on Geoscience and Remote Sensing, 48 (1): 547-555. doi: http://dx.doi.org/10.1109/TGRS.2009.2024934.

Cui L., Li G., Ren H., He L., Liao H., Ouyang N., Zhang Y. (2014) - *Assessment of atmospheric correction methods for historical Landsat TM images in the coastal zone: A case study in Jiangsu, China*. European Journal of Remote Sensing, 47: 701-716. doi: http://dx.doi.org/10.5721/EuJRS20144740.

Dominguez A., Kleissl J., Luvall J.C., Rickman D.L. (2011) - *High-resolution urban* thermal sharpener (*HUTS*). Remote Sensing of Environment, 115 (7): 1772-1780. doi: http://dx.doi.org/10.1016/j.rse.2011.03.008.

Gioli B., Miglietta F., Vaccari F.P., Zaldei A., De Martino B. (2006) - *The Sky Arrow ERA, an innovative airborne platform to monitor mass, momentum and energy exchange of ecosystems*. Annals of Geophysics, 49: 109-116. doi: http://dx.doi.org/10.4401/ag-3159.

Gluch R., Quattrochi D.A., Luvall J.C. (2006) - *A multi-scale approach to urban thermal analysis*. Remote Sensing of Environment, 104: 123-132. doi: http://dx.doi.org/10.1016/j.rse.2006.01.025.

Jimenez-Munoz J.C., Cristobal J., Sobrino J.A., Soria G., Ninyerola M., Pons X. (2009) - *Revision of the single-channel algorithm for land surface temperature retrieval from Landsat thermal-infrared data*. IEEE Transaction on Geoscience and Remote Sensing, 47 (1): 339-349. doi: http://dx.doi.org/10.1109/TGRS.2008.2007125.

Jimenez-Munoz J.M., Sobrino J.A., Gillepse A.R. (2012) - *Surface emissivity retrieval from airborne Hyperspectral scanner data: insights on atmospheric correction and noise removal*. IEEE Geoscience and Remote Sensing Letters, 9 (12): 180-184. doi: http://dx.doi.org/10.1109/LGRS.2011.2163699.

Hancock R.N., Torgesen C.E, Cherkauer K.A., Gillespie A.R, Tockner K., Faux R.N., Tan J. (2012) - *Thermal Infrared remote sensing of water temperature in riverine landscapes*. Fluvial Remote Sensing for Science and Managenment: 85-113, Carbonneau P.E.,

Piegay J. (Eds). Available online at: http://faculty.washington.edu/cet6/pub/Handcock_etal_2012.pdf.

Hartz D.A., Prashad L., Hedquist B.C., Golden J., Brazel A.J. (2006) - *Linking satellite images and hand-held infrared thermography to observed neighborhood climate conditions.* Remote Sensing of Environment, 104: 190-200. doi: http://dx.doi.org/10.1016/j.rse.2005.12.019.

Inamdar A.K., French A., Hook S., Vaughan G., Luckett W. (2008) - *Land surface temperature retrieval at high spatial and temporal resolutions over the southwestern United States*. Journal of Geophysical Research, 113 (D7): 1-18. doi: http://dx.doi.org/10.1029/2007JD009048.

Kottmeier C., Biegert C., Corsmeier U. (2007) - *Effects of Urban Land Use on Surface Temperature in Berlin: Case Study.* Journal of Urban Planning and Development, 133 (2): 128-137. doi: http://dx.doi.org/10.1061/(ASCE)0733-9488(2007)133:2(128).

Kustas W.P., Norman J.M., Anderson M.C., French A.N. (2003) - *Estimating subpixel surface temperatures and energy fluxes from the vegetation index-radiometric temperature relationship*. Remote Sensing of Environment, 85: 429-440. doi: http://dx.doi.org/10.1016/S0034-4257(03)00036-1.

Lee H.Y. (1993) - *An application of NOAA AVHRR thermal data to the study of urban heat islands*. Atmospheric Environment, 27 (1): 1-13, doi: http://dx.doi.org/10.1016/0957-1272(93)90041-4.

Li Y., Zhang H., Kainz W. (2012) - *Monitoring patterns of urban heat islands of the fast-growing Shanghai metropolis, China: Using time-series of Landsat TM/ETM+ data*. International Journal of Applied Earth Observation and Geoinformation, 19: 127-138. doi: http://dx.doi.org/10.1016/j.jag.2012.05.001.

Lo C.P., Quattrochi D.A, Luvall J.C. (1997) - *Application of high-resolution thermal infrared remote sensing and GIS to assess the urban heat island effect*. International Journal of Remote Sensing, 18: 287-304. doi: http://dx.doi.org/10.1080/014311697219079.

Lu D., Weng Q. (2006) - *Spectral mixture analysis of ASTER images for examining the relationship between urban thermal features and biophysical descriptors in Indianapolis, Indiana, USA.* Remote Sensing of Environment, 104: 157-167. doi: http://dx.doi.org/10.1016/j.rse.2005.11.015.

Mitraka Z., Chrysoulakis N., Kamarianakis Y., Partsinevelos P., Tsouchlaraki A. (2012) - *Improving the estimation of urban surface emissivity based on sub-pixel classification of high resolution satellite imagery*. Remote Sensing of Environment, 117: 125-134. doi: http://dx.doi.org/10.1016/j.rse.2011.06.025.

Mukherjee S., Joshi P.K., Garg R.D. (2015) - *Regression-Kriging technique to downscale satellite-derived land surface temperature in heterogeneous landscape*. IEEE Journal of Selected Topics in Applied Earth Observations and Remote Sensing, 8 (3): 1245-1250. doi: http://dx.doi.org/10.1109/JSTARS.2015.2396032.

National Aeronautics and Space Administration (NASA) (1999) - *MODIS UCSB emissivity library*. Available online at: http://www.icess.ucsb.edu/modis/EMIS/html/em.html.

Oke T.R. (1973) - *City size and the urban heat island.* Atmospheric Environment, 7: 769-779. doi: http://dx.doi.org/10.1016/0004-6981(73)90140-6.

Oke T.R. (1982) - *The energetic basis of the Urban Heat Island*. Quarterly Journal of the Royal Meteorological Society, 108: 1-24. doi: http://dx.doi.org/10.1002/

qj.49710845502.

Pu R., Gong P., Michishita R., Sasagawa T. (2006) - *Assessment of multi-resolution and multi-sensor data for urban surface temperature retrieval*. Remote Sensing of Environment, 104: 211-225. doi: http://dx.doi.org/10.1016/j.rse.2005.09.022.

Saaaroni H., Ben-Dor E., Bitan A., Potcher O. (2000) - *Spatial distribution and microscale characteristics of the urban heat island in Tel-Aviv, Israel*. Landscape and Urban Planning, 48: 1-18. doi: http://dx.doi.org/10.1016/S0169-2046(99)00075-4.

Sobrino J.A., Jimenez-Munoz J.C., Paolini L. (2004) - *Land surface temperature retrieval from LANDSAT TM 5.* Remote Sensing of Environment, 90: 434-440. doi: http://dx.doi.org/10.1016/j.rse.2004.02.003.

Sobrino J.A., Oltra-Carrió R., Sòria G., Bianchi R., Paganini M. (2012) - *Impact of spatial resolution and satellite overpass time on evaluation of the surface urban heat island effects*. Remote Sensing of Environment, 117: 50-56. doi: http://dx.doi.org/10.1016/j.rse.2011.04.042.

Stathopoulou M., Cartalis, C. (2009) - *Downscaling AVHRR land surface temperatures for improved surface urban heat island intensity estimation*. Remote Sensing of Environment, 113: 2592-2605. doi: http://dx.doi.org/10.1016/j.rse.2009.07.017.

Streutker D.R. (2003) - *Satellite-measured growth of the urban heat island of Houston, Texas*. Remote Sensing of Environment, 85 (3): 282-289. doi: http://dx.doi.org/10.1016/S0034-4257(03)00007-5.

Voogt J.A., Oke T.R. (1998) - *Effects of urban surface geometry on remotely-sensed surface temperature*. International Journal of Remote Sensing, 19: 895-920. doi: http://dx.doi.org/10.1080/014311698215784.

Voogt J.A. (2004) - *Urban Heat Island: Hotter Cities*. ActionBioscience.org. Available online at: http://www.actionbioscience.org/environment/voogt.html.

Xian G., Crane M. (2006) - *An analysis of urban thermal characteristics and associated land cover in Tampa Bay and Las Vegas using Landsat satellite data*. Remote Sensing of Environment, 104: 147-156. doi: http://dx.doi.org/10.1016/j.rse.2005.09.023.

Xiong Y., Huang S., Chen F., Ye H., Wang C., Zhu C. (2012) - *The Impacts of Rapid Urbanization on the Thermal Environment: A Remote Sensing Study of Guangzhou, South China*. Remote Sensing, 4: 2033-2056. doi: http://dx.doi.org/10.3390/rs4072033.

Xu H. (2007) - *Extraction of urban built-up land features from Landsat Imagery using a Thematic-oriented index combination technique*. Photogrammetric Engineering & Remote Sensing, 73 (12): 1381-1391. doi: http://dx.doi.org/10.14358/PERS.73.12.1381.

Xu H., Ding F., Wen X. (2009) - *Urban Expansion and Heat Island Dynamics in the Quanzhou Region, China*. IEEE Journal of Selected Topics in Applied Earth Observations and Remote Sensing, 2 (2): 74-79. doi: http://dx.doi.org/10.1109/JSTARS.2009.2023088.

Yuan F., Bauer M.E. (2007) - *Comparison of impervious surface area and normalized difference vegetation index as indicators of surface urban heat island effects in Landsat imagery*. Remote Sensing of Environment, 106 (3): 375-386. doi: http://dx.doi.org/10.1016/j.rse.2006.09.003.

Weng Q., Hu X., Quattrochi D.A., Liu H. (2014) - *Assessing Intra-Urban Surface Energy*

Fluxes Using Remotely Sensed ASTER Imagery and Routine Meteorological Data: A Case Study in Indianapolis, U.S.A. IEEE Journal of Selected Topics in Applied Earth Observations and Remote Sensing, 7 (10): 4046-4057. doi: http://dx.doi.org/10.1109/JSTARS.2013.2281776.